Supporting Information

Chemical Vapor Deposition of Mesoporous Graphene Nano-Balls for Supercapacitor

Jung-Soo Lee†, Sun-I Kim†, Jong-Chul Yoon, and Ji-Hyun Jang*

Interdisciplinary School of Green Energy, Low Dimensional Carbon Materials Center and KIER-UNIST Advanced Center for Energy, UNIST, Korea

† These authors contributed equally to this work

Materials

Styrene, Methacrylic acid, Potassium persulfate, PVP, Sulfuric acid, and $FeCl_3$ were purchased from Aldrich Co and used without any further purification.

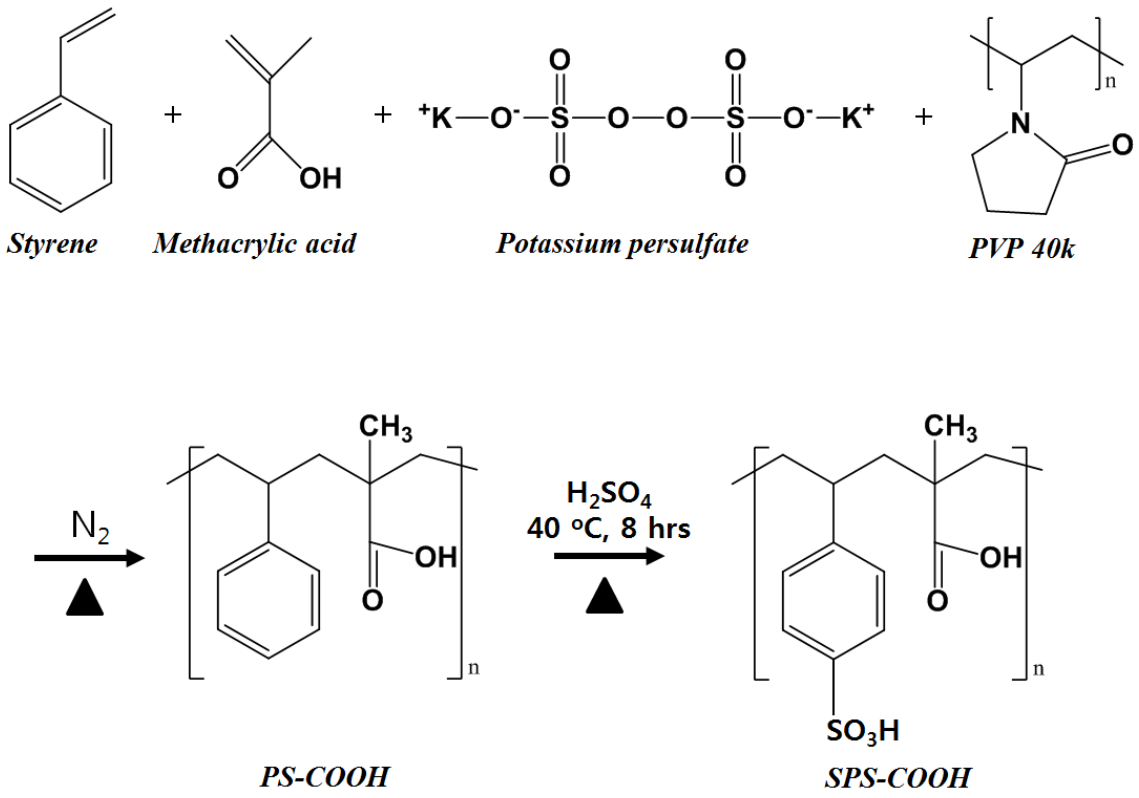

Figure S1. Emulsion polymerization procedure for synthesis of sulfonated poly (styrene-co-methacrylic acid) (SPS-COOH).

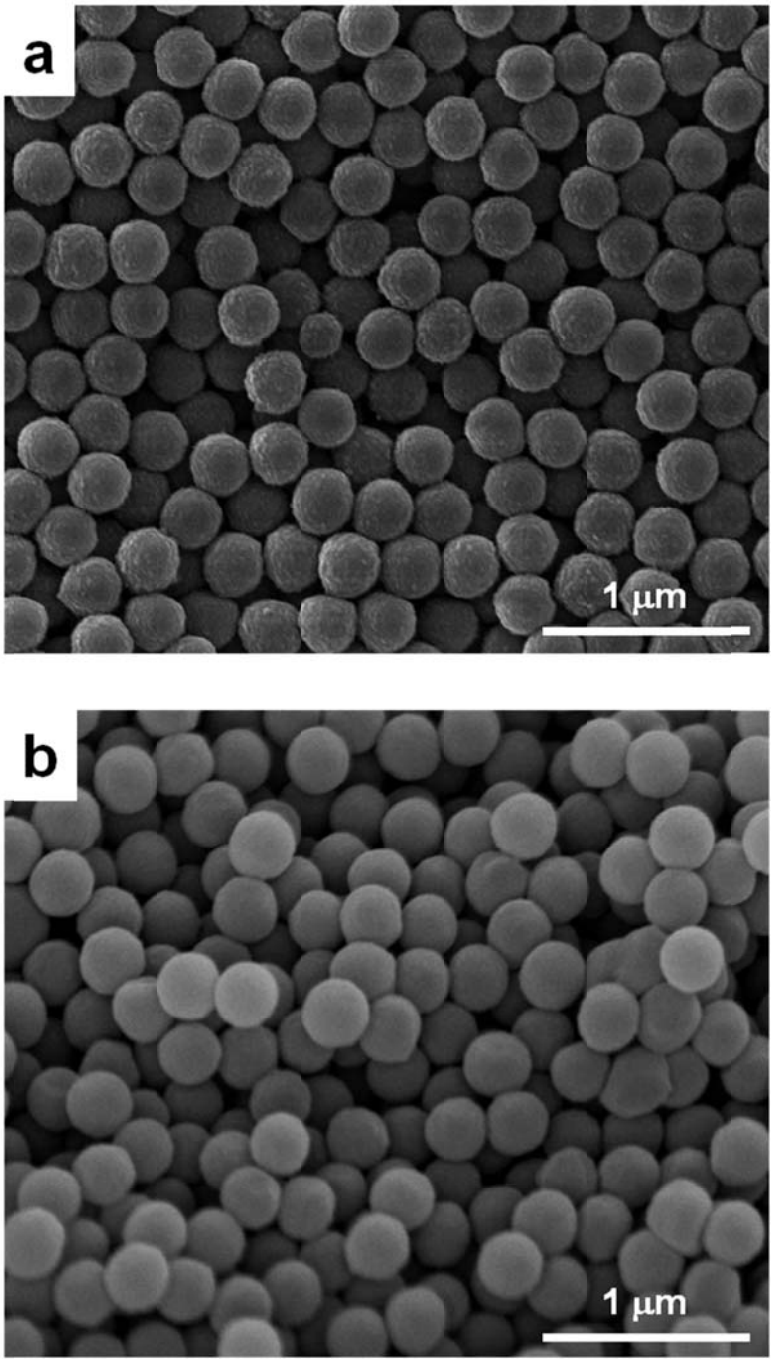

Figure S2. SEM images of (a) PS-COOH and (b) SPS-COOH.

The rough morphology of the PS-COOH surface is likely due to the hydrophilic poly methacrylic acid chain being rolled up due to the difference in polarity from the hydrophobic surface of the PS sphere (Figure S2a). After sulfonation of PS-COOH, the surface

morphology becomes smooth as shown in Figure S2b.

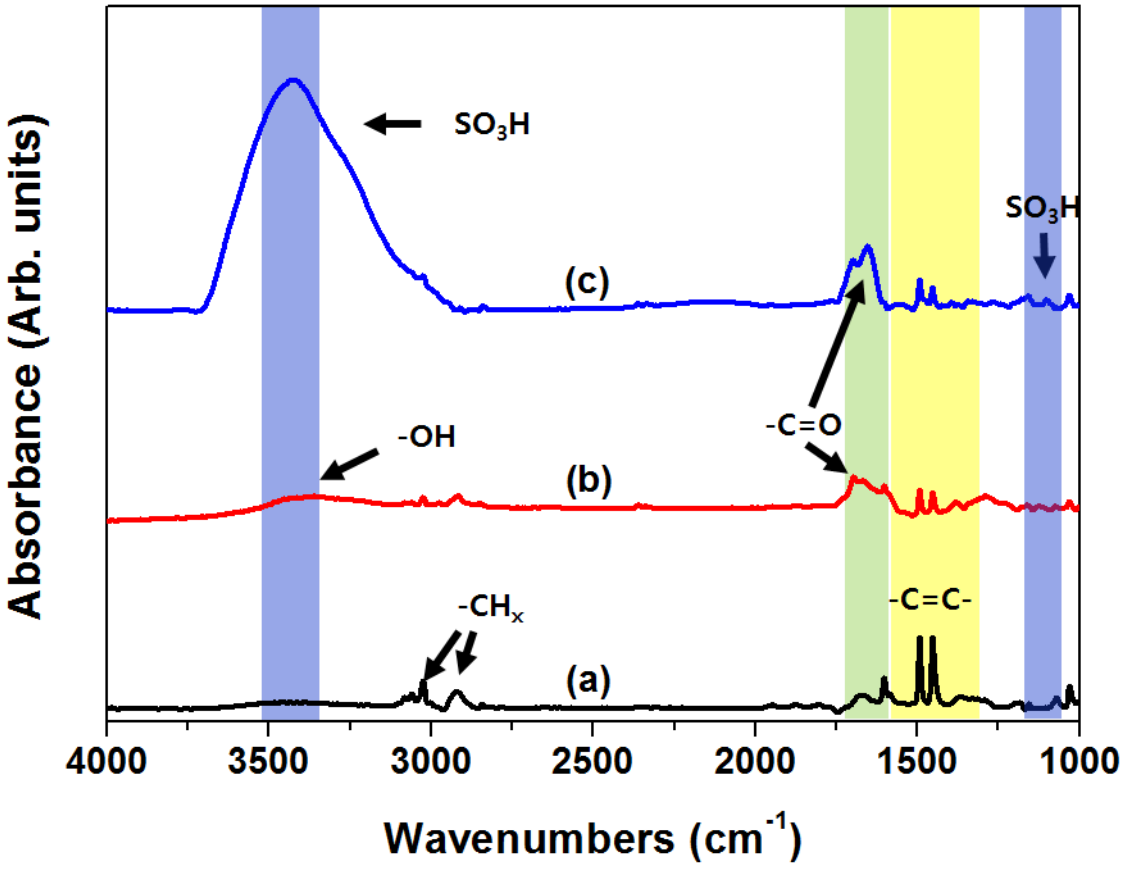

Figure S3. FT-IR analysis of (a) PS, (b) PS-COOH, and (c) SPS-COOH

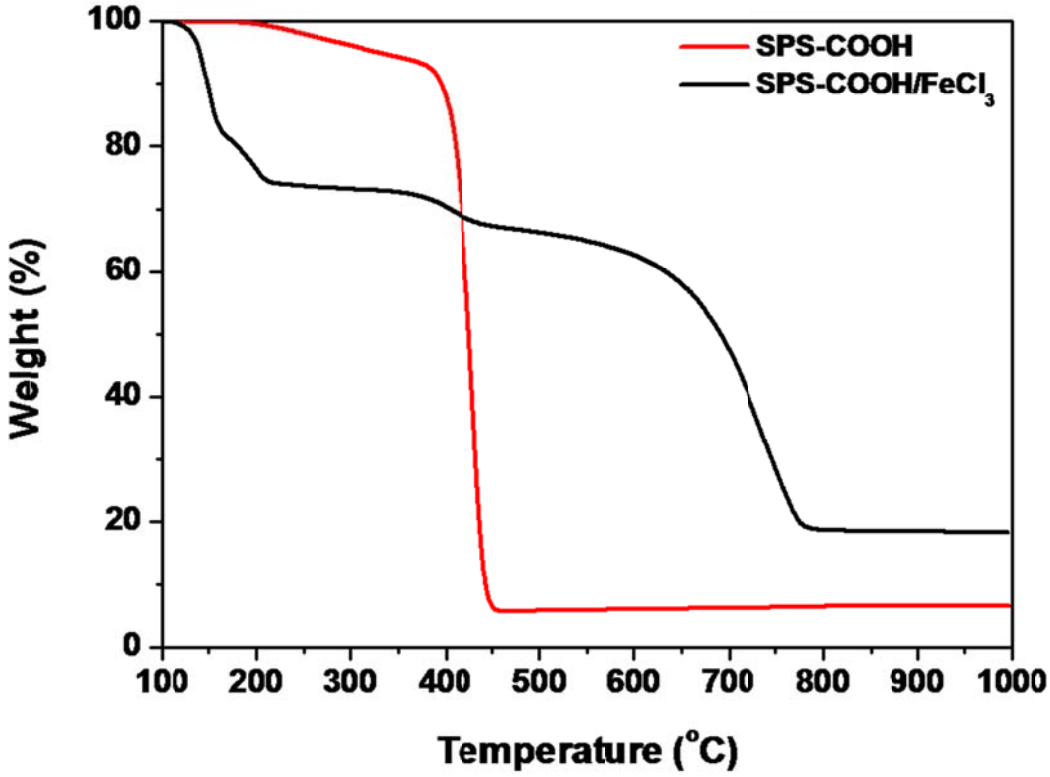

Figure S4. TGA analysis of SPS-COOH and SPS-COOH/$FeCl_3$

Titration

A SO_3H/COOH ratio in SPS-COOH was obtained from the value of ion exchange capacity (IEC), which can be determined by titration. 0.4 g of each sample was dispersed in 50 ml of 1 M NaCl solutions and stirred for 1 day for complete exchange of H^+ ions in SPS-COOH with Na^+. The HCl solutions created from ion exchange reactions were titrated with 0.1 M NaOH. The ratio of –COOH to $–SO_3H$ in SPS-COOH is calculated to be 1:0.68 from the value of ICE of PS-COOH and SPS-COOH.

$$IEC = \frac{f \cdot V \cdot M}{W}$$

Where, f = Factor =1
V = Volume of NaOH (ml)
M = Mol of NaOH (ml)
W = Weight of dried sample

-COOH, -SO_3H + 1M NaCl ➔ -COONa, -SO_3Na + HCl ➔ Titration with 0.1M NaOH

a

	PS-COOH	SPS-COOH
IEC (μmol/g)	8.56	14.4

b

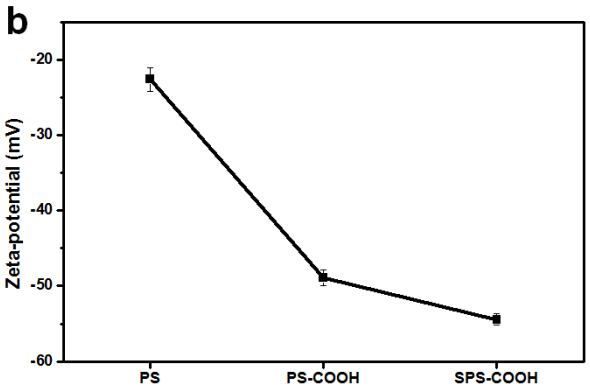

Figure S5. (a) IEC of PS-COOH and SPS-COOH. (b) Zeta potential of PS, PS-COOH, and SPS-COOH. The stronger ionic strength of $–SO_3H$ functional group than –COOH functional groups leads to stronger negative Zeta-potential of SPS-COOH.

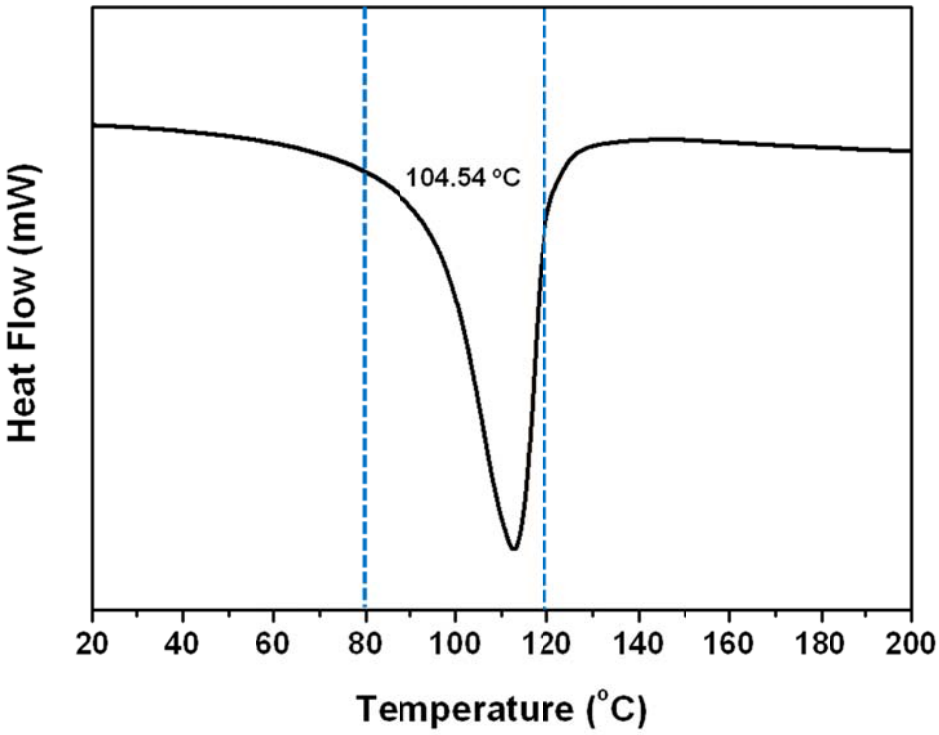

Figure S6. DSC analysis of SPS-COOH

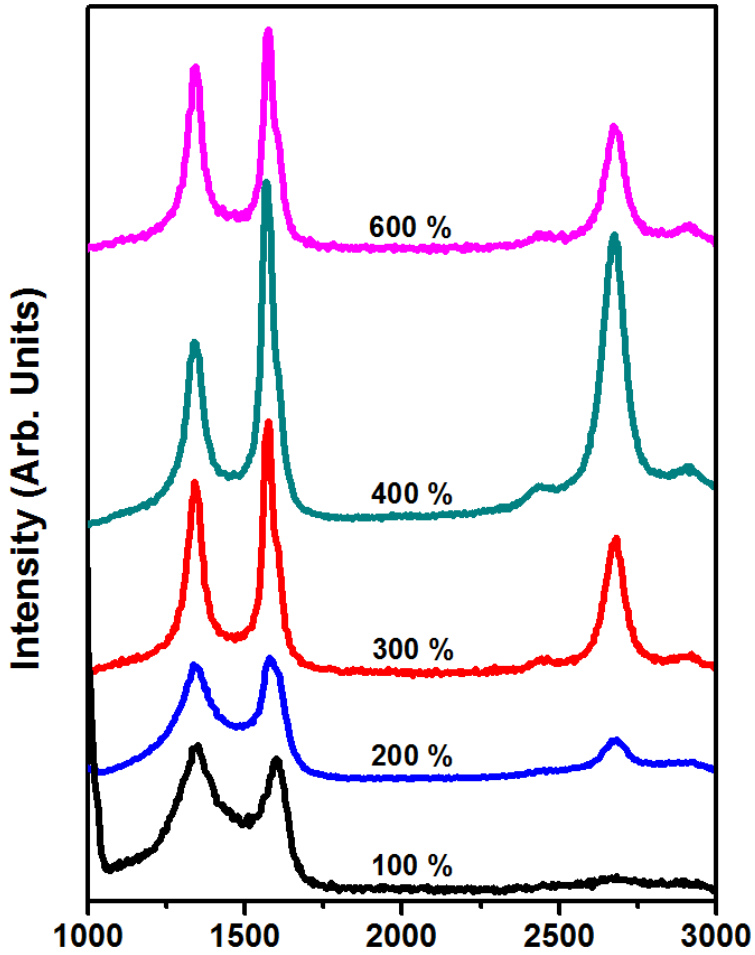

Figure S7. Raman spectra of MGB grown by precursor-assisted CVD with various composition ratios of $FeCl_3 \cdot 6H_2O$ to SPS-COOH

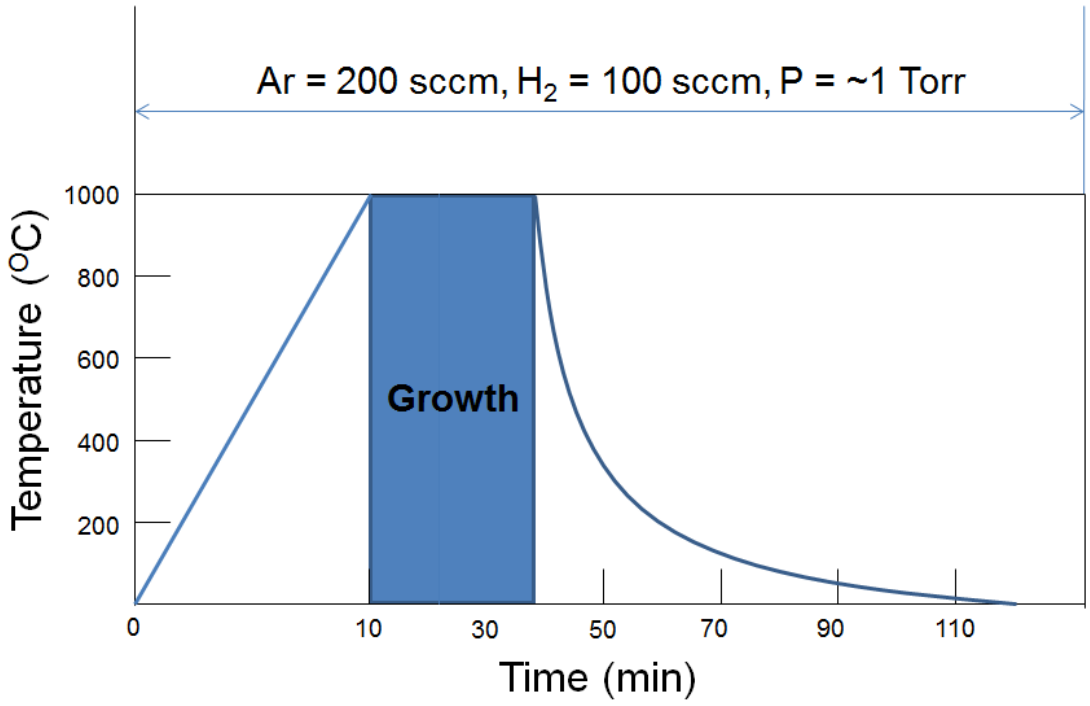

Figure S8. Schematic diagram of the process for the growth of MGB via precursor assisted CVD.

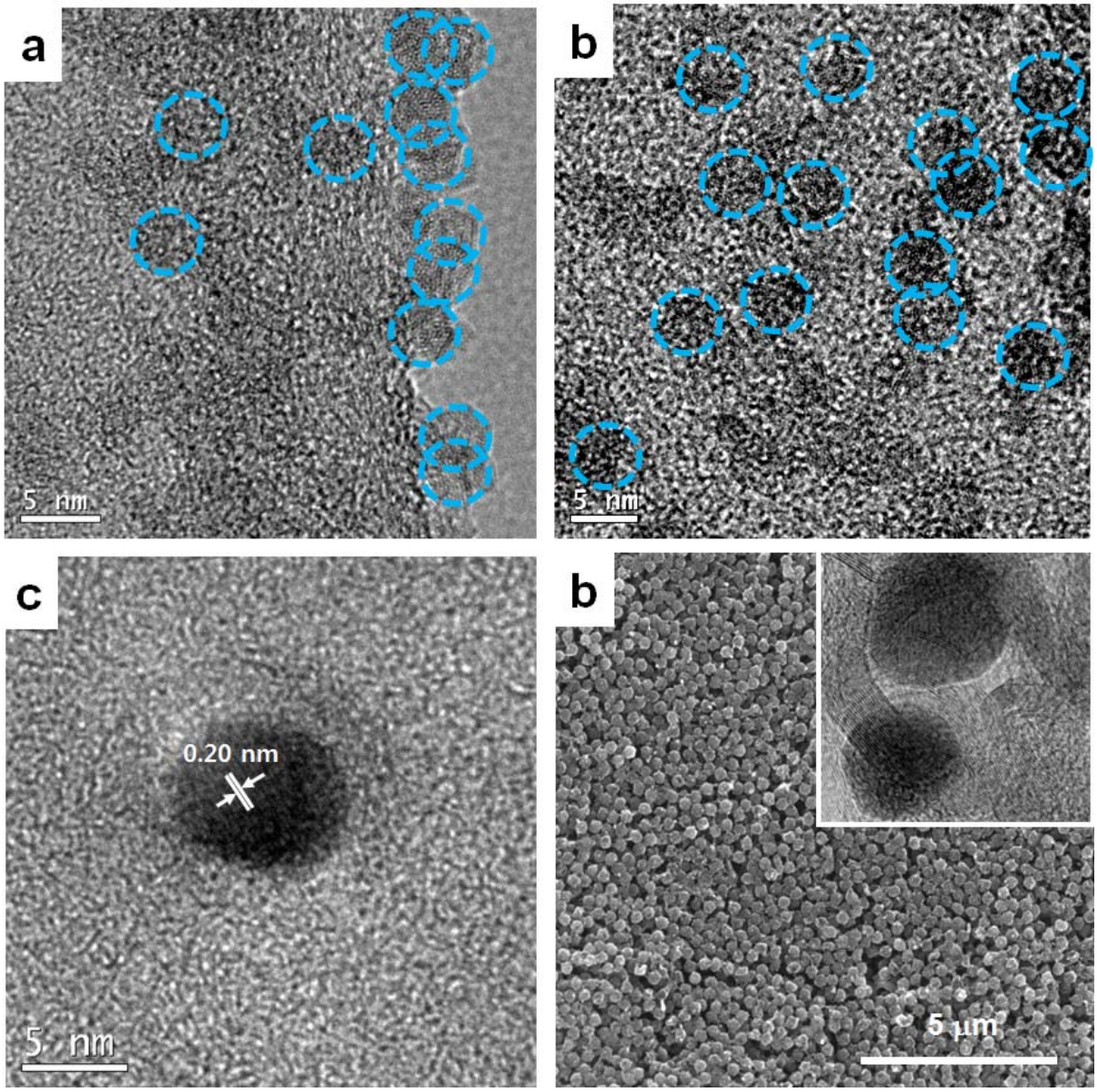

Figure S9. TEM images of MGB before the removal of Fe particles in different areas. (a) Aggregated Fe particles on the surface of PS balls. (b) Fe particles inside PS balls. (c) Fe nanoparticle with a diameter of 4.5 nm. (d) Large scale SEM image of densely packed MGB/Fe. The inset presents MGB created on the surface of Fe nanoparticles.

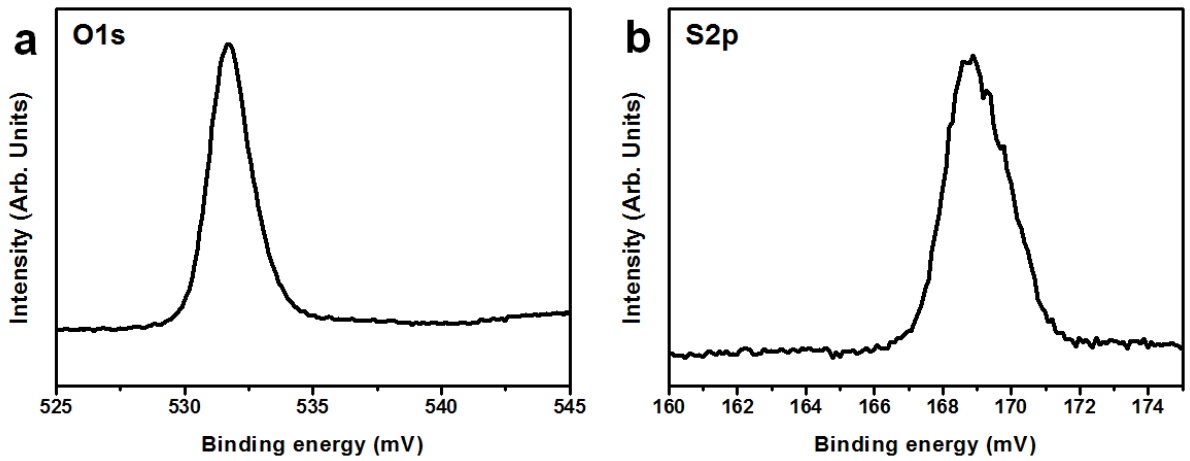

Figure S10. XPS analysis of p-doped MGBs : O1s peak (a) and S2p peak (b).

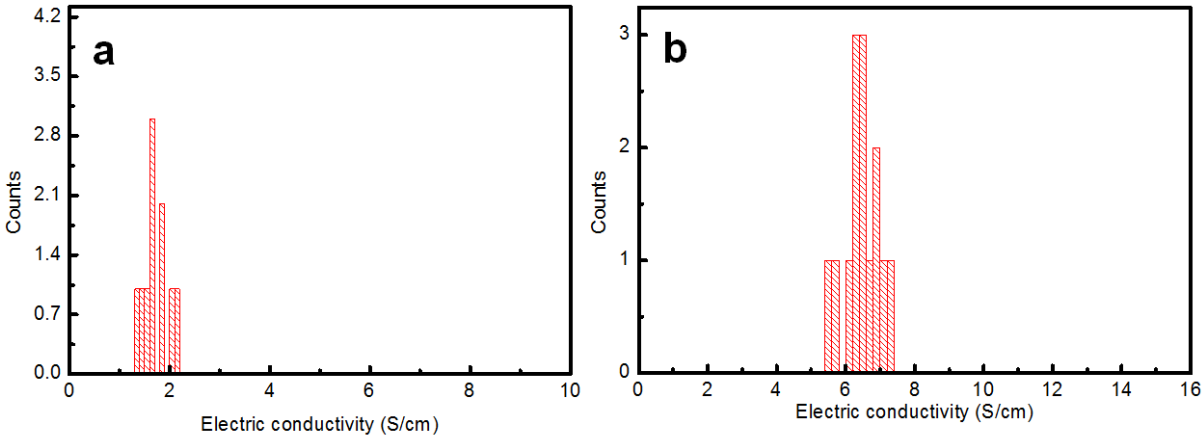

	N total	Mean	Standard Deviation	Sum	Minimum	Median	Maximum
MGBs	10	1.71	0.258	17.14	1.38	1.63	2.17
p-doped MGBs	14	6.48	0.49921	90.72148	5.47705	6.45833	7.28757

Figure S11. Conductivity analysis of MGBs (a) and p-doped MGBs (b)

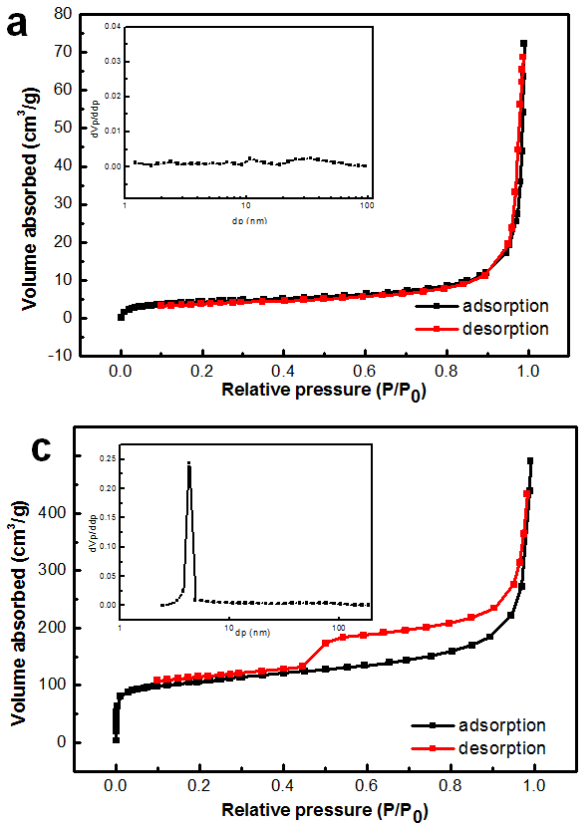

	Surface area (m^2 g^{-1})	Pore volume (Cm^3 g^{-1})	$d_{p,peak}$ (nm)
PS balls	15.152	0.1063	33.81
MGB	508	0.74	4.27
p-doped MGB	346.08	0.757	4.27

Figure S12. BET analysis of PS (a), MGB (b), and p-doped MGB (c).

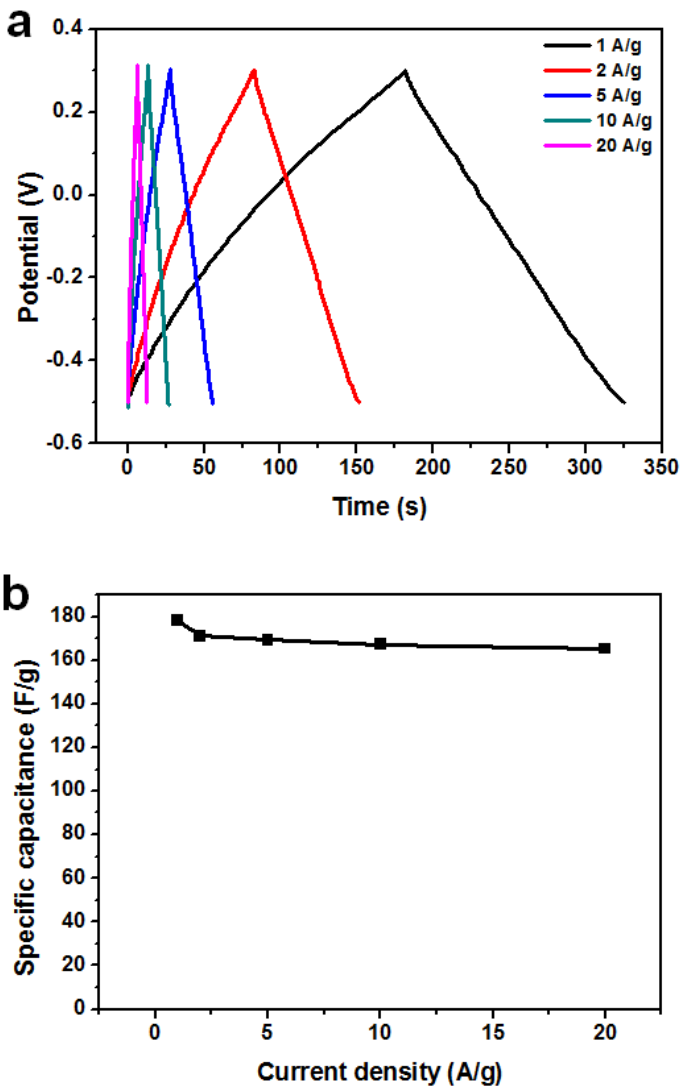

Figure S13. (a) Charge/discharge curves of p-doped MGB with increasing time. Symmetric charge/discharge curves indicate MGB-based ideal capacitor properties. (b) Specific capacitance of p-doped MGB at various current densities.